This is a preprint, the final version is subject to change, of the American Mineralogist (MSA)
Cite as Authors (Year) Title. American Mineralogist, in press.
(DOI will not work until issue is live.) DOI: http://dx.doi.org/10.2138/am-2017-5825

Revision 2

Column anion arrangements in chemically zoned ternary chlorapatite and fluorapatite from Kurokura, Japan

SEAN R. KELLY[1*], JOHN RAKOVAN[1]

[1]Department of Geology and Environmental Earth Science, Miami University, Oxford, Ohio 45056, U.S.A.

JOHN M. HUGHES[2]

[2]Department of Geology, University of Vermont, Burlington, Vermont 05405, U.S.A.

ABSTRACT

The substitution of F, OH and Cl in apatite has recently gained increased attention due to the complex nature of incorporation of these three constituents and the implications of apatite column anion chemistry, such as apatite's contribution to the water budget of the moon and Mars and the use of apatite anion chemistry as an indicator of halogen and water activities. The solid solutions among F, OH, and Cl are complex because the end-member atomic arrangements cannot fully explain the ternary and binary substitutions of these constituents due to differing atomic radii and the resulting steric constraints in the structure. Three structural variations have recently been reported for the OH-Cl binary solid solution in synthetic samples. This study elucidates column anion arrangements in a chemically zoned ternary apatite from Kurokura, Japan. The structures of the compositionally different core and rim were solved (R1=0.0158 and R1=0.0143, respectively) in space group $P6_3/m$ using single crystal X-ray diffraction data. The chemistry of these apatites was analyzed using electron microprobe analysis and crystal structure refinement. The core of the Kurokura crystal is a naturally occurring example of the OH ≈ Cl

*Email: Seanrkelly11@gmail.com

apatite structural variation in a ternary chlorapatite, with four column anion sites (one for F, two for Cl and one for *both* OH and Cl). The rim exhibits a previously unseen apatite structural variation in a ternary OH-rich fluorapatite (with only a trace Cl component) with three column anion sites (one each for F, OH and Cl). Both structural variations show a splitting of the Ca2 site that enables reasonable column anion bond distances with Ca2 atoms. A sequence of anions that provides reasonable anion-anion distances while simultaneously enabling reversal of the anion sites relative to the mirror planes at $z = 1/4$ and $z = 3/4$ exists for both structure variations. This study demonstrates the structural complexity of natural ternary apatites, and that a structural variety of OH-Cl apatite occurs over a wider range of chemistry than initially anticipated. The results have implications regarding the poorly understood (and potentially complex) crystallization history of apatite from Kurokura, Japan.

Keywords: apatite, ternary solid solution, chlorapatite, Kurokura, Japan

INTRODUCTION

Apatite *sensu lato* [$Ca_{10}(PO_4)_6(OH,F,Cl)_2$; OH = hydroxylapatite, F = fluorapatite, Cl = chlorapatite], the most abundant phosphate mineral on Earth, plays an important role across many disciplines (Hughes and Rakovan 2002; Hughes and Rakovan 2015; Rakovan and Pasteris 2015). Hydroxylapatite is the closest naturally occurring analog to bone material, and new insights about the occurrence of OH in bone apatite have recently been reported (Pasteris et al. 2014). Apatite is also one of the more common hydroxyl-bearing phases in extraterrestrial systems, such as the moon and Mars (McCubbin and Jones 2015; McCubbin et al. 2010a; Boyce et al. 2010). Boyce et al. (2014) recently suggested that apatite plays the dominant role in fractionation of F, OH, and Cl in lunar magmatic systems. Understanding the structure and

thermodynamic properties of apatite will allow better estimation of the overall H_2O content within extraterrestrial magmatic systems from measured apatite chemistries.

The F, OH, and Cl chemical variation in apatite can also provide a variety of geochemical information. One example is using apatite anion chemistry as a geothermometer (*e.g.*, Stormer and Charmichael 1971). Apatite anion chemistry can also serve as an indication of magma or aqueous fluid composition from which the phase crystallized (Piccoli and Candela 2002), including the fugacity of volatiles in magmatic, metamorphic, or hydrothermal systems (Webster and Piccoli 2015; McCubbin et al. 2015; Hughes et al. 1990; Yardley 1985).

Chlorapatite, an uncommon naturally occurring apatite phase, is unique in that it can indicate rather unusual mineralization environments where it is found. For example, experimental work has suggested that Cl-rich apatite may be chemically associated with Pt in mineralizing hydrothermal fluids, demonstrating the significance of apatite anion chemistry to mineral exploration (Webster and Piccoli 2015).

As noted by Hughes et al. (2016), for any combination of anion occupants, the positions of the anions in the [0,0,*z*] anion column result from several factors, including the size of the particular column anions, the nearest-neighbors in the anion column and electrostatic repulsions therefrom, any dissymmetrization (lowering of crystal symmetry) that is present in the structure, electrostatic attractions to the surrounding triangle of Ca2 atoms, and, in hydroxyl-bearing apatite, the hydrogen bonding that occurs from the hydroxyl hydrogen to neighboring column anions. Figure 1 shows a [001] projection of the apatite atomic arrangement. Because of the steric flexibility of its structure, apatite can incorporate a large range of (F, Cl, OH) compositions in the anion column sites.

Hughes et al. (1989) published one of the most recent structural analyses of the OH, F, and Cl end members of the ternary system of anion substitution. Apatite most commonly crystallizes in space group $P6_3/m$, although subsymmetric varieties are known (Hughes and Rakovan 2015). In end-member fluorapatite, the F anion resides at (0, 0, 0.25) and (0, 0, 0.75) in the unit cell, lying on {001} mirror planes at $z = 1/4$ and $z = 3/4$. The larger OH and Cl (poly)anions are usually displaced off this mirror plane (*ca*. 0.3 and 1.3Å, respectively), a structural response to steric interaction with the surrounding Ca cations (the Ca2 position, see Figure 1), which also lie on the mirror planes. Figure 1 demonstrates the configuration of calcium anions surrounding the column anion. Although the substitution of these three anions is known to be extensive, the continuous solution series of these anions cannot be explained by their end-member atomic sites alone (Hughes et al. 1990).

It has been shown that novel, non-end member atomic sites exist in the ternary solution series as well as the binary F-Cl and OH-Cl solution series (Hughes et al. 1990, 2014a, 2014b, 2016). Hughes et al. (1990) also demonstrated in natural samples that ternary solid solution can occur *via* ordering of OH and Cl atoms, causing symmetry reduction to $P2_1/b$. The F-OH apatite binary can exist with the end-member F and OH sites while maintaining $P6_3/m$ symmetry, as the smaller radii of these (poly)anions enable disorder about the mirror planes without necessitating new sites (Hughes et al. 1989). Hughes et al. (2016) recently demonstrated, in a series of synthetic apatites, that three different structures with distinctly different column anion sites enable solid solution along the OH-Cl binary series without reduction of symmetry due to ordering. The structure of OH-Cl apatites is influenced by column anion chemistry, with one arrangement for apatites with OH dominant, one for apatites with approximately equal OH and Cl *apfu*, and one for apatites with Cl dominant in the anion column. The calcium phosphate

apatite structure preferentially incorporates F over both OH and Cl (Boyce et al. 2014). In order for natural apatite dominated by OH and Cl to exist, crystal growth must have occurred from a fluid or magma substantially devoid of F relative to OH or Cl. This study presents the structure and chemistry of a natural Cl- and OH-dominant calcium phosphate apatite from Kurokura, Ashigarakami district, Kanagawa Prefecture, Japan, and an analysis of the column anion arrangement. These apatites occur in hydrothermal veins in diorite and granodiorite, in association with quartz, chlorite, talc, stilbite, and natrolite. Crystals are prismatic with well-developed {100} {001} {101} faces and are typically 0.5-1.0 cm in length, but can exceed 4 cm (Figure 2). Apatites from Kurokura were first reported to be chlorine dominant by Harada (1938). Apatites from this locality consist of two visually distinct concentric zones: a volumetrically dominant clear core and a white (cloudy) rim (Figure 2). The rim is cloudy due to a high density of small fluid inclusions (note: the larger 'bubbles' in this image occur in the epoxy rather than the mineral; the fluid inclusions in the rim are much smaller). Harada (1938) demonstrated both optically and with wet chemical analysis that the cloudy rim and clear core represent two distinct apatite chemistries. Apatite from the core is more Cl rich than that from the rim. This concentric chemical zoning may be indicative of variation in source fluid chemistry during apatite crystallization, or possibly post-growth alteration of the rim. Although the chemical analysis of Harada (1938) suggests that both the core and rim contain significant F, preliminary investigation in this study suggested that one or both of these phases is OH-rich chlorapatite.

EXPERIMENTAL

Single crystal x-ray diffraction (SCXRD) was used as a crystal structure analysis technique and chemical probe of the apatite samples from Kurokura in this study. There are some

instances, however, where different anions are shown to occupy the same column site (Hughes et al. 2014a, 2016), causing a limitation in the accuracy of this methodology. Electron microprobe analysis (EMPA) was employed as a complementary technique for analysis of the F and Cl chemistry. Measuring O with EMPA is known to be problematic; OH chemistry is instead calculated by difference, assuming two column (poly)anions per unit cell. This method of determining OH chemistry is not ideal, particularly given the known limitations of measuring F and Cl by microprobe analysis (discussed below).

Electron microprobe analysis

A sample of Kurokura apatite was prepared for EPMA analysis by embedding the crystal in epoxy resin and slicing to achieve a (100) section. The sample was then progressively polished down to a 0.02 μm alumina paste. Measuring the Cl and F composition of apatite using EPMA is known to be problematic (Stormer et al. 1993; Stock et al. 2015), as column anion migration can lead to spurious results. One way to reduce column anion migration is to use (100) sections for analysis (Stormer et al. 1993). Six spots were measured on the polished sample, three within the clear core and three within the white rim.

Compositional analyses were acquired on a Cameca SX100 electron microprobe, at the University of Oregon's CAMCOR MicroAnalytical facility, equipped with 5 tunable wavelength-dispersive spectrometers. A 15 keV accelerating voltage and 20 nA beam current were used for measurement of Ca, F, Cl, P, and Fe, and a 20 keV accelerating voltage and a 50 nA beam current were used for measurement of S, Nd, Na, Sr, Ce, Mn, Si, Dy, and Eu. The beam size was 10 microns for all analyses. Elemental analyses were acquired using the following analyzing crystals: LIF (Fe, Dy, Eu), PET (Ca, S, Nd, Si, P), LPET (Ce, Mn, Cl), and LTAP (Sr, F, Na). The standards used were synthetic MnO (Mn), SrTiO3 (Sr), synthetic chlorapatite

(halogen corrected) (P, Ca, Cl), nepheline (partial anal.) (Na, Si), magnetite (Fe), pyrite (S), BaF_2 (F), $CePO_4$ (Ce), $DyPO_4$ (Dy), $EuPO_4$ (Eu), and $NdPO_4$ (Nd). The counting time was 60 seconds for F, Cl, Fe, S, Nd, Na, Sr, Ce, Mn, Dy, and Eu, 90 seconds for P and Ca, and 120 seconds for Si. The intensity data were corrected for time dependent intensity (TDI) loss (or gain) using a self-calibrated correction for Ca, F, Cl, P, and Fe. This correction accounts for the known variation of F and Cl peak intensity over time in apatite due to anion migration. The off-peak counting time was 30 seconds for Ca and P, 60 seconds for Cl, F, Fe, S, Nd, Na, Sr, Ce, Mn, Dy, and Eu, and 120 seconds for Si. Interference corrections were applied to F (P, Ce, Eu and Nd), Cl (Nd), Nd (Ce and Eu), Sr (Si), Ce (Sr), Mn (Nd and Eu), Dy (Mn, Eu, and Fe), and Eu (Mn and Nd). Oxygen was calculated by cation stoichiometry and included in the matrix correction. Oxygen-equivalence from halogens (F/Cl/Br/I), was not subtracted in the matrix correction. Hydrogen was calculated by difference. Further details of the EMPA experimental methods used in this study can be found in Armstrong (1988) and Donovan et al. (1993; 2011).

Single crystal X-ray diffraction

X-ray diffraction data were collected with a Bruker Apex II CCD single-crystal diffractometer using graphite-monochromated Mo K_α radiation; complete details of crystal data and data collection for each of the two crystals described herein have been deposited.[3] For each sample, redundant data were collected for a sphere of reciprocal space (4,500 frames, 0.20º scan width, average redundancy ≈ 16) and were integrated and corrected for Lorentz and polarization factors and absorption using the Bruker Apex2 package of programs. The atomic arrangement

[3] Deposit items AM-xx-xx1 for crystal data and data collection and AM-xx-xx2 for CIF files. Deposit items are available two ways: for paper copies contact the Business Office of the Mineralogical Society of America (see inside front cover of recent issue) for price information. For an electronic copy visit the MSA web site at http://www.minsocam.org, go to the *American Mineralogist* Contents, find the table of contents for the specific volume/issue wanted, and then click on the deposit link there.

was refined in space group $P6_3/m$, on F^2, with SHELXL-97 (Sheldrick 2008) using neutral atom scattering factors and full-matrix least-squares, minimizing the function $\Sigma\, w(F_o^2 - F_c^2)^2$ with no restraints. All atoms were refined with anisotropic temperature factors except the column anions. As noted previously (e.g., Hughes et al. 1990a, 2014a, 2016) use of anisotropic atomic displacement factors for the column anions yields unreasonable values of U_{33}, an anisotropy that masks the positions of anion sites occupied by small fractions of a column anion. The occupancy values of the column anions were not constrained.

After structure solution and initial refinement, the column anion positions were analyzed by difference maps. In this way, positions along the anion column were modeled and refined one at a time, as they sequentially appeared as the highest peaks in the difference maps. Disorder of the Ca2 site was also modeled in this fashion, as sites Ca2 and Ca2'. When disorder of the Ca2 site was modeled, the sum of the Ca2 and Ca2' site occupancy was constrained to total 1.00 and the two sites were also constrained to have identical thermal parameters. An extinction coefficient was also refined in both samples. Using previous literature, anion positions were named and assigned an anion scattering factor (Cl, O, or F). Anion selection was then evaluated using the calculated total anion *apfu* based on the refinement.

RESULTS

Electron microprobe analysis

Table 1 shows the chemistry results from EMPA data for each portion of the crystal. Figure 3 shows the column anion chemistry results from each of the six individual analysis spots, as well as average anion chemistry for the core and two averages for the rim. The average core anion chemistry is $[Cl_{0.93}\ (OH)_{0.66}\ F_{0.38}]$ and the average rim anion chemistry is $[F_{0.97}\ (OH)_{0.88}$

182 $Cl_{0.24}$]. As determined by Harada (1938), the apatite core has a higher Cl concentration than the
183 rim. Figure 3 demonstrates a notable presence of column anion chemical heterogeneity in the
184 Kurokura apatite, particularly in the rim. One of the three spots where rim chemistry was
185 measured has anion values much more similar to the core than the other two rim spots (Figure 3;
186 see labeled outlier spot). Although this may simply represent heterogeneity in the rim, the outlier
187 may also be the result of collecting data across the boundary between the core and rim. Because
188 of this possibility, an average rim chemistry from EMPA analysis not including the outlier is also
189 shown in Figure 3. Comparison of EMPA data to anion chemistry determined by crystal
190 structure analysis is given below.

191 **Crystal structure refinements**

192 The structures of the clear apatite core and cloudy rim were solved and refined using
193 SCXRD data to R1 values of 0.0158 and 0.0143, respectively. Both samples were successfully
194 modeled in space group $P6_3/m$. Tables 2 and 3 contain the atomic coordinates and equivalent
195 atomic displacement parameters for the core and rim, respectively. From the refined atomic
196 arrangement, the core anion chemistry is $[Cl_{0.87}\ (OH)_{0.58}\ F_{0.55}]_{\Sigma 2.00}$ and the rim apatite's chemistry
197 is $[F_{1.05}\ (OH)_{1.02}\ Cl_{0.04}]_{\Sigma 2.12}$. These results are plotted on Figure 3, alongside the results from
198 EMPA. There is some disagreement between anion chemistry determined by SCXRD and
199 EMPA, primarily for the rim sample. This difference may be the result of analytical error,
200 particularly with EMPA due to the known limitations in quantifying F and Cl (and the inability
201 to measure OH). The discrepancy may also be in part due to heterogeneity in the samples; the
202 data from EMPA and SCXRD were collected on different individual crystal fragments.

203 The clear core has the same column anion arrangement reported in Hughes et al. (2016)
204 that exists for OH-Cl apatites with OH occupancy approximately equal to Cl occupancy in the

anion column. Conversely, the cloudy rim was found to have a new column anion arrangement for ternary apatites that are predominantly F and OH. The column anion arrangements of each zone of the crystal are discussed further below.

Clear apatite core

Four anion column sites were refined for the sample of the clear core portion of the Kurokura apatite, yielding a column anion arrangement almost identical to the Cl ≈ OH apatite structure published in Hughes et al. (2016). The position and occupancy of the four sites are given in Table 4.

Two distinct Cl sites were found at $z = 0$ and $z = 0.094$. The site at $z = 0$ represents a unique Cl position only found in binary F-Cl and OH-Cl calcium phosphate apatites (Hughes et al. 2014; 2016). The site at $z = 0.094$ is nearly equivalent to the Cl atomic site in end-member chlorapatite, only slightly less displaced from the mirror planes at $z = 1/4$ and $z = 3/4$ than the typical end member Cl site ($z \approx 0.068$; Hughes et al. 1989). This site has an acceptable bond distance to Ca2' of 2.878Å.

Another column anion site was found in the clear apatite core samples at $z = 0.166$. This site is particularly interesting, having only recently been documented in Hughes et al. (2016). As is the case in Hughes et al. (2016), here it is demonstrated that this site represents a special site with mixed occupancy of *both* OH and Cl.

In order for OH and Cl (poly)anions with significantly different radii (Cl = 1.72Å, OH = 1.33Å; Jenkins and Thakur 1979) to occupy the same atomic site, they must both achieve acceptable bond distances with the neighboring Ca2 site. This requires the splitting of the Ca2 site into two distinct sites, which was found in this structure refinement (Ca2 and Ca2'; Table 2). The ClOH site has a distance of 2.387Å to the Ca2 site (acceptable for OH) and 2.637Å to the

Ca2' site (acceptable for Cl). These interatomic distances are almost identical to those found in Hughes et al. (2016) (2.404Å to Ca2 and 2.647Å to Ca2'). Further supporting mixed occupancy of the site at $z = 0.166$ is that the sum of the site occupancies of the column anions (which should be approximately 2 anions per unit cell) is substantially *below* 2.00 when the ClOH site is modeled as Cl (1.70 atoms per unit cell) and substantially *above* 2.00 when the ClOH site is modeled as OH (2.39 atoms per unit cell). Because of this, as in Hughes et al. (2016), a total column occupancy of 100% (2.00 atoms per unit cell) was used to calculate the proportion of the ClOH site occupied by each anion (Table 4).

A final site was found at $z = 1/4$, directly centered among three Ca2 cations on the mirror plane at $z = 1/4$ and $z = 3/4$ and concordant with the F position in end-member fluorapatite. However, Hughes et al. (2016) found that in their synthetic apatite where OH ≈ Cl (with anion sites identical to those published here) OH can occupy this site. Dual occupancy of this site by F and OH makes fractional occupancy determination *via* SCXRD difficult, because the scattering factors of O^{2-} and F^{-} are nearly identical as they are isoelectronic. However, EMPA data from the Kurokura core (Table 1; Figure 3) indicates 16-23% F occupancy of the anion column. This occupancy coincides closely with the refined site occupancy at $z = 1/4$ in the structure (28% occupied, Table 4), suggesting that this site is exclusively (or almost exclusively) occupied by F in the Kurokura core. No OH was modeled at this site in the refinements. This demonstrates that the OH ≈ Cl apatite structural result found in Hughes et al. (2016) occurs over a wider range of apatite anion chemistry than just in the OH-Cl binary, and that this structure variant, i.e. column anion arrangement, is found in nature.

For this apatite sample to maintain the hexagonal symmetry of space group of $P6_3/m$, it must be demonstrated that a sequence of atoms exists, given the refined atomic sites in the anion

column, to reverse the ordering of sites from above the mirror planes at z = 1/4 and z = 3/4 to below these mirror planes, such that throughout the crystal the occupancies are averaged half above and half below. Hughes et al. (2016) proposed a model for reversal of the anion column with acceptable anion-anion distances for this particular apatite structure. This model is shown in Figure 4, with the only difference being F occupancy of the site at z = 1/4 and 3/4. The c dimension of the structure from this paper is only 0.002 Å larger than that used in the model from Hughes et al. (2016), and the interatomic distances are effectively identical. As mentioned in Hughes et al. (2016), OH must occupy the Cla and Clb site in trace quantities to enable this reversal sequence. Given the constraints proposed in Mackie and Young (1974): (1) the interatomic distances between occupants of the anion column must be of reasonable length, 2) the anions must occupy positions found in the structure refinement, and 3) F [and OH] can occupy a Cl site but Cl cannot occupy an F [or OH] site because of the resulting short Ca-Cl distances, it is reasonable to propose that *both* F and OH can occupy the Cla and Clb sites (F and OH are both smaller than Cl), making reversal of the anion column *via* the sequence in Figure 4 possible.

White apatite rim

The structure of the white outer rim of the apatite crystal (Figure 2) was found to have three column anion sites, with the overall chemistry being that of a OH-rich fluorapatite (almost identical OH and F concentrations) with a small chlorine component. The unit cell fractional coordinates of these column anion sites and their occupancy factors are given in Table 5.

One column anion site was modeled at z = 1/4, identical to the end-member fluorapatite column site. This site is considered here to be occupied by F, as with the core refinement there is no reason to suggest it is occupied by OH. The EMPA data demonstrate high F in the apatite rim

(Table 1), supporting the occupancy of the $z = 1/4$ site by F. Another site was refined at $z = 0.19$. This was modeled as an OH site, as it is close to the end-member hydroxylapatite column site ($z \approx 0.20$, Hughes et al. 1989). A third site was modeled at $z = 0.11$, which is slightly less offset from the mirror planes at $z = 1/4$ and $z = 3/4$ than the end-member chlorapatite site ($z \approx 0.068$). This site was modeled as a Cl site.

A splitting of the Ca2 site into Ca2 and Ca2' was also modeled in this sample. The F and OH sites have acceptable bond distances to the Ca2 site of 2.32Å and 2.35Å, respectively. The Cl site is prohibitively close to the Ca2 site (2.51Å), but has an acceptable bond distance of 2.79Å to the Ca2' site, making the Ca2' site a necessary component of this apatite structure. The short Ca2' to O2 distance (2.11 Å) indicates the requirement of an O2' site for the Ca2' site to be feasible. The highest peak in the difference map (0.51 $e^-/Å^3$) is an O2' site that when modeled provides an acceptable Ca2'-O2' distance (2.39 Å), affirming the O2 disorder. However, the data could not successfully support the modeling of disordered O2 and the concomitant disordering of P, and thus it was not modeled.

The combined column anion site occupancy refined to 2.12 sites per unit cell, slightly over the 2.00 sites per unit cell mandated by the apatite structure. This indicates a potential inaccuracy in the refinement. One possible explanation for the over occupancy of the anion column in the rim refinement is that there is Cl occupying the OH or F site that is not being accounted for in the model. The interatomic distances between the Ca2' site and the F/OH sites (Ca2'-OH: 2.66Å; Ca2'-F: 2.63Å) are both large enough to ideally accommodate Cl. This suggests that there may be a small amount of Cl occupancy in either (or both) the F and OH sites (more likely the OH site) that is accounting for the over occupancy of the anion column in the model. Adding Cl occupancy at the F and OH sites moves the SCXRD anion chemistry closer to

297 the anion chemistry determined by EMPA, as EMPA found substantially more Cl than SCXRD
298 (2.1% vs. 12% of total column occupancy, respectively). However, the very small occupancy of
299 the Ca2' site (3.49% occupied) suggests that only a very small amount of substitution of Cl into
300 the OH or F sites may be occurring, if any. As mentioned in Hughes et al. (2016), there should
301 be a 1:1 linear relationship between the occupancy of the Ca2' site and the occupancy of the
302 column anion sites that require the Ca2' site to have reasonable bond distances. The Cl site in
303 this structure is 2.12% occupied, leaving 1.37% possible occupancy of the F and OH sites by Cl.

304 This apatite column anion arrangement has not previously been documented. However,
305 comparison below demonstrates that the structure may represent a low Cl analog to the
306 hexagonal structure of a ternary apatite collected from "ash F" in the Gunnison Formation near
307 Jackson Peak, southwestern Utah, published in Hughes et al. (1990). That structure has identical
308 F and OH sites, as well as splitting of the Ca2 site (with a short 2.16Å Ca2'-O2 distance). The
309 only structural difference is that, unlike the structure published here, Hughes et al. (1990)
310 documented a splitting of the Cl site into two: one at $z = 0.132$ and another at $z = 0.06$. Splitting
311 of the Cl site was proposed due to the abnormally large U_{33} value (0.098Å). The U_{eq} value for the
312 Cl site in the rim structure in this paper is not unusually large (0.01045), and thus a split is not
313 considered. A key difference that likely explains this observation is the different chemistry of
314 these apatites.

315 The apatite described herein is approximately a pure binary F-OH apatite, with only 0.04
316 Cl atoms per unit cell. The small occupancy on the Cl site in this structure provides uncertainty
317 as to the legitimacy of the site. The site was included in the model, however, due to EMPA data
318 showing substantial Cl, the presence of the Ca2' site, and that removal of the Cl site from the

refinement leads to a higher R value (0.0149) and the appearance of an electron density peak of 0.64 $e^-/Å^3$ in the difference map near $z = 0.10$ (near the Cl site).

The ternary apatite from Hughes et al. (1990) has a much higher Cl occupancy of 0.63 Cl atoms per unit cell. The greater proportion of Cl in the apatite from Hughes et al. (1990) may be what causes the splitting of the Cl site. Furthermore, a greater Cl occupancy can also make it easier to resolve a splitting of the Cl site. The very low Cl occupancy of the Kurokura rim structure is effectively a limitation in observing this split if it does exist.

A model demonstrating a possible reversal of the column anion occupancy necessary to maintain $P6_3/m$ symmetry using the sites found in this study is shown in Figure 5. As seen in Figure 5, the most prohibitive anion-anion distance necessary to enable disorder of anion sites from one side of the mirror plane at $z = 1/4$ and $z = 3/4$ to the other is an OH-Cl distance of 2.89Å. This distance is greater than an OH-Cl distance proposed in Hughes et al. (2016) (2.85Å), and is considered acceptable.

IMPLICATIONS

This study presents two structural variations of apatite, within compositionally different concentric zones of the same crystal, which have previously not been documented in natural samples. Whereas a naturally occurring OH-Cl binary apatite was not found, the clear core portion of these apatite crystals represents the first naturally occurring example of the OH ≈ Cl OH-Cl apatite structure variety first published in Hughes et al. (2016). The fact that this structure was found in an apatite with a significant F component demonstrates that this structural result occurs over a wider range of apatite chemistries than documented in Hughes et al. (2016) using pure Cl-OH synthetic crystals. The rim represents an F- and OH-dominant ternary apatite with a

new structural variety closely resembling previously documented hexagonal ternary apatite (Hughes et al. 1990).

The distinct difference in chemistry from the core and rim suggests that the two zones of the crystal represent either two distinct mineralization events/fluids or one mineralization event that was later metasomatically altered. The rim representing an alteration phase is consistent with the substantial chemical heterogeneity of the rim observed in the microprobe data (Figure 3).

Further investigation will be necessary for addressing the petrological questions posed herein. New analyses, such as an elemental map documenting the chemistry variation over a section of a crystal, or analysis of the fluid inclusions present in the rim, may elucidate the cause of the anion chemistry variation from the rim to the core. Understanding the petrogenic history of this apatite is pertinent to the interpretation of these results from a petrological standpoint. It is possible that the two different apatite structural varieties presented here are affected both by variation in chemistry (evident given the difference in anion chemistry in each phase) and variation in temperature, particularly given the possibility that the rim may represent a lower temperature alteration of the original apatite phase.

There is little background literature on the crystallization events of the Kurokura region, making it impossible to put the work of this paper into the context of the greater geology of Kurokura. Further studies of this region will help to better characterize the unique formation conditions responsible for formation of apatite at Kurokura.

ACKNOWLEDGEMENTS

Support for this work was provided by the National Science Foundation through grant EAR-1249459 to JMH and EAR-0952298 to JR. Reviews by Francis McCubbin, Jill Pasteris, and an anonymous reviewer improved this manuscript significantly.

365 **REFERENCES**

366 Armstrong, J.T. (1988) Quantitative analysis of silicate and oxide materials: comparison of
367 Monte Carlo, ZAF, and phi-rho-z procedures. Microbeam Analysis, 239-246.
368 Boyce, J.W., Liu, Y., Rossman, G.R., Guan, Y., Eiler, J.M., Stolper, E.M., and Taylor, L.A.
369 (2010) Lunar apatite with terrestrial volatile abundances. Nature Letters, 466, 466-469.
370 Boyce J.W., Tomlinson S.M., McCubbin, F.M., Greenwood, J.P., and Treiman, A.H. (2014)
371 The Lunar Apatite Paradox. Science, 344, 400–402.
372 Donovan, J.J., Lowers, H.A, and Rusk, B.G. (2011) Improved electron probe microanalysis of
373 trace elements in quartz. American Mineralogist, 96, 274–282.
374 Donovan, J.J., Snyder, D.A., and Rivers, M.L. (1993) An Improved Interference Correction for
375 Trace Element Analysis. Microbeam Analysis, 2, 23-28.
376 Harada, Z. (1938) Beiträge zur Kenntnis der optischen und chemischen Eigenschaften de Apatits
377 von Kurokura, Kanagawa Präfektur. Journal of the Faculty of Science, Hokkaido
378 Imperial University. Ser. 4, Geology and mineralogy, 4, 11-16. (in German)
379 Hughes, J.M., and Rakovan, J. (2002) The Crystal Structure of Apatite, $Ca_5(PO_4)_3(F,OH,Cl)$. In
380 Kohn, M., J.F. Rakovan & J.M. Hughes, Eds., Phosphates: Geochemical, Geobiological
381 and Materials Importance, 48, p. 1-12. Reviews in Mineralogy and Geochemistry,
382 Mineralogical Society of America, Chantilly, Virginia.
383 Hughes, J.M., and Rakovan, J. (2015) Structurally robust, chemically diverse: Apatite and apatite
384 supergroup minerals. Elements, 11, 167-172.
385 Hughes, J.M., Cameron, M., and Crowley, K.D. (1989) Structural variations in natural F, OH
386 and Cl apatites. American Mineralogist, 74, 870-876.

Hughes, J.M., Cameron, M., and Crowley, K.D. (1990) Crystal structures of natural ternary apatites: solid solution in the $Ca_5(PO_4)_3X$ (X = F, OH, Cl) system. American Mineralogist, 75, 295-304.

Hughes, J.M., Nekvasil, H., Ustunisik, G., Lindsley, D.H., Coraor, A.E., Vaughn, J., Phillips, B., McCubbin, F.M., and Woerner, W.R. (2014a) Solid solution in the fluorapatite - chlorapatite binary system: High-precision crystal structure refinements of synthetic F-Cl apatite. American Mineralogist, 99, 369-376.

Hughes, J.M., Heffernan, K.M., Goldoff, B., and Nekvasil, H. (2014b) Fluor-chlorapatite, devoid of OH, from the Three Peaks Area, Utah: The first reported structure of natural fluor-chlorapatite. Canadian Mineralogist, 52, 643-652.

Hughes, J.M., Harlov, D.H., Kelly, S.R., Rakovan J., Wilke, M. (2016) Solid solution in the apatite OH-Cl binary system: compositional dependence of solid solution mechanisms in calcium phosphate apatites along the Cl-OH binary. American Mineralogist, 101, 1783-1791.

Jenkins, H.D.B., and Thakur, K.P. (1979) Reappraisal of thermochemical radii for complex anions. Journal of Chemical Education, 56, 576-577.

Mackie, P.E., and Young, R.A. (1974) Fluorine-chlorine interaction in fluor-chlorapatite. Journal of Solid State Chemistry, 11, 319-329.

McCubbin, F.M. and Jones, R.H. (2015) Extraterrestrial Apatite: Planetary Geochemistry to Astrobiology. Elements. 11, 183-188.

McCubbin, F.M., Steele, A., Hauri, E.H., Nekvasil, H., Yamashita, S., and Hemley, R.J. (2010) Nominally hydrous magmatism on the Moon. Proceedings of the National Academy of Science, 107, No 25, 11223-11228.

McCubbin, F.M., Vander Kaaden, K.E., Tartese, R., Boyce, J.W., Mikhail, S., Whitson, E.S., Bell, A.S., Anand, M., Franchi, I.A., Wang, J.H. and Hauri, E.H. (2015) Experimental investigation of F, Cl, and OH partitioning between apatite and Fe-rich basaltic melt at 1.0-1.2 GPa and 950-1000 oC. American Mineralogist 100, 1790-1802.

Pasteris J.D., Yoder, C.H., and Wopenka, B. (2014) Molecular water in nominally unhydrated carbonated hydroxylapatite: The key to a better understanding of bone mineral. American Mineralogist, 99, 16–27.

Piccoli, P.M., and Candela, P.A. (2002) Apatite in Igneous Systems. In Kohn, M., J.F. Rakovan & J.M. Hughes, Eds., Phosphates: Geochemical, Geobiological and Materials Importance, 48, p. 255-292. Reviews in Mineralogy and Geochemistry, Mineralogical Society of America, Chantilly, Virginia.

Rakovan, J., and Pasteris J.D. (2015) A Technological Gem: Materials, Medical, and Environmental Mineralogy of Apatite. Elements, 11, 195-200.

Sheldrick, G.M. (2008) A short history of SHELX. Acta Crystallographica, A64, 112–122.

Stock, M.J., Humphreys, M.C.S., Smith, V. C., Johnson, R.D., Pyle, D.M., and EIMF (2015) New constraints on electron beam induced halogen migration in apatite. American Mineralogist, 100, 281-293.

Stormer, J.C., and Carmichael, I.S.E. (1971) Fluorine-hydroxyl exchange in apatite and biotite: A potential igneous geothermometer. Contributions to Mineralogy and Petrology, 3l, l2l-131.

Stormer, J.C., Pierson, M.L., and Tacker, R.C. (1993) Variation of F and Cl X-ray intensity due to anisotropic diffusion in apatite during electron microprobe analysis. American Mineralogist, 78, 641–648.

Webster, J.D., Piccoli, P.M. (2015) Magmatic Apatite: A Powerful, Yet Deceptive, Mineral. Elements, 11, 167-172.

Yardley, B.W.D. (1985) Apatite composition and the fugacities of HF and HCI in metamorphic fluids. Mineralogical Magazine, 49, 77-79.

This is a preprint, the final version is subject to change, of the American Mineralogist (MSA)
Cite as Authors (Year) Title. American Mineralogist, in press.
(DOI will not work until issue is live.) DOI: http://dx.doi.org/10.2138/am-2017-5825

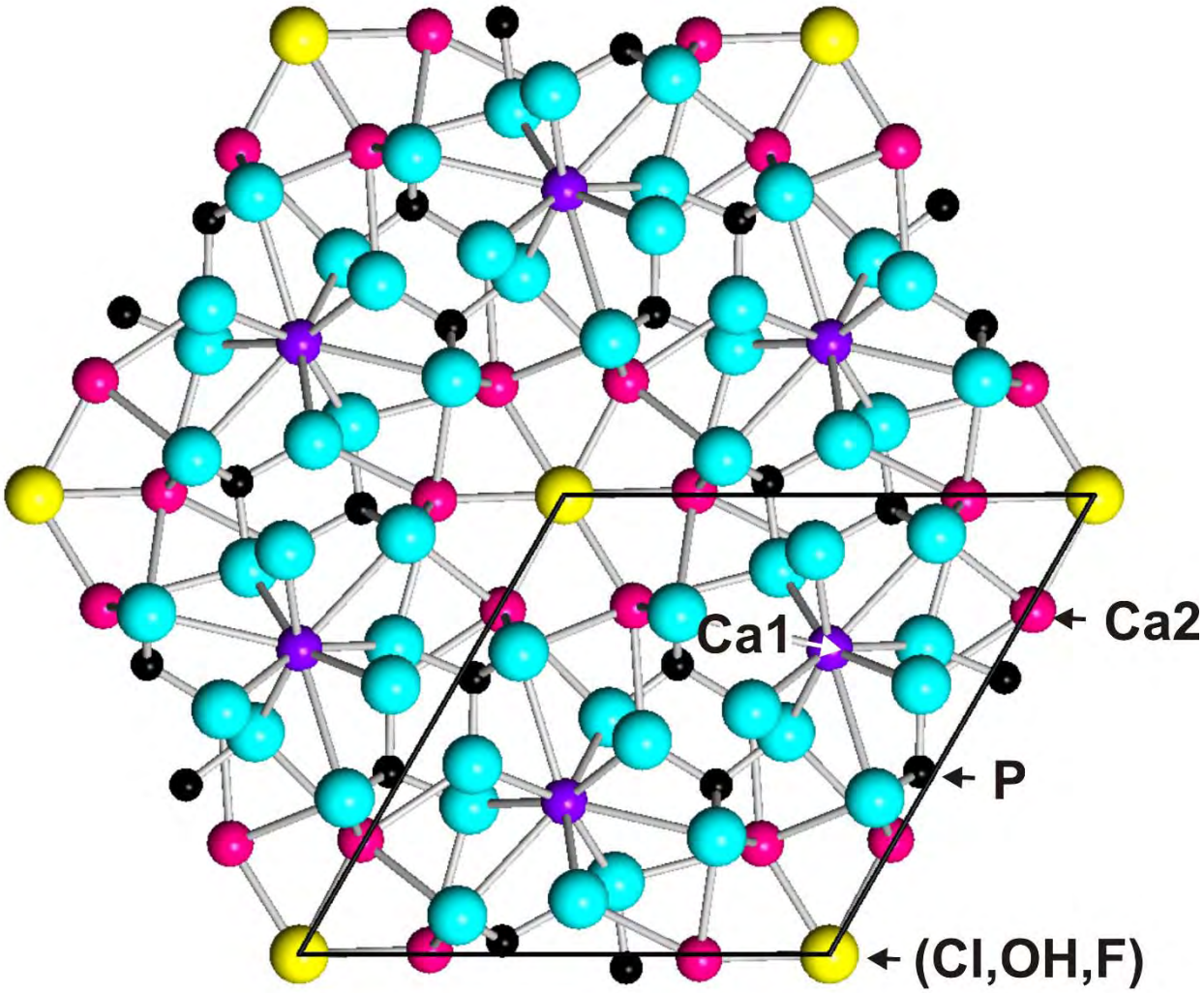

FIGURE 1. (001) projection of the crystal structure of apatite.

This is a preprint, the final version is subject to change, of the American Mineralogist (MSA)
Cite as Authors (Year) Title. American Mineralogist, in press.
(DOI will not work until issue is live.) DOI: http://dx.doi.org/10.2138/am-2017-5825

FIGURE 2a. A 1.2 cm tall single crystal of apatite from Kurokura, Ashigarakami district, Kanagawa Prefecture, Japan.

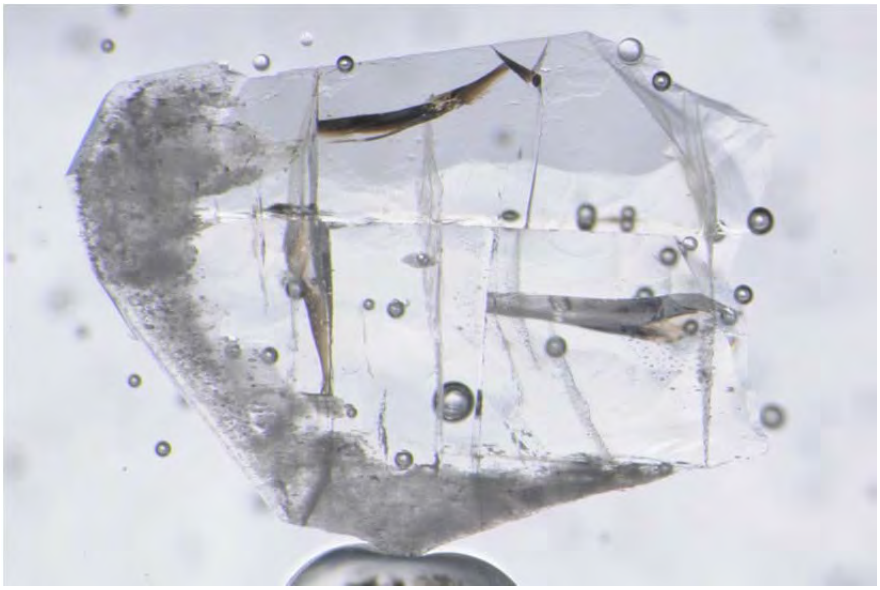

FIGURE 2b. Transmitted light image of the polished Kurokura apatite (100) section used for EMPA. Both the clear core portion of the crystal and the white, cloudy rim of the crystal are seen. The field of view in this image is approximately 5mm across. The larger

bubbles seen throughout the image are air bubbles trapped in the epoxy. The sample is approximately 2 mm thick.

FIGURE 2c. Approximately 1 cm tall Kurokura apatite crystals demonstrating the white rim and clear, colorless core.

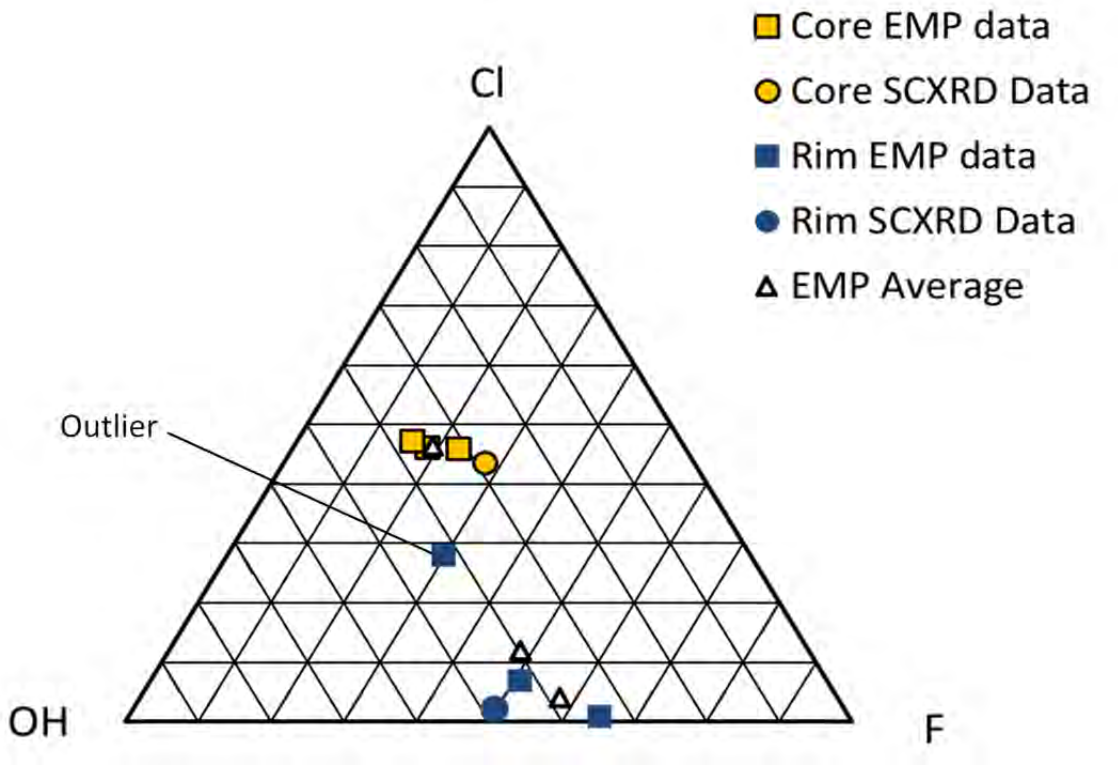

FIGURE 3. Ternary plot of the column anion chemistry (percent of total column occupancy) of the apatite rim and core from both structure refinement (SCXRD data) and electron microprobe analysis. Two averages for the rim EMPA column anion chemistry are shown, one including the outlying data point and one without.

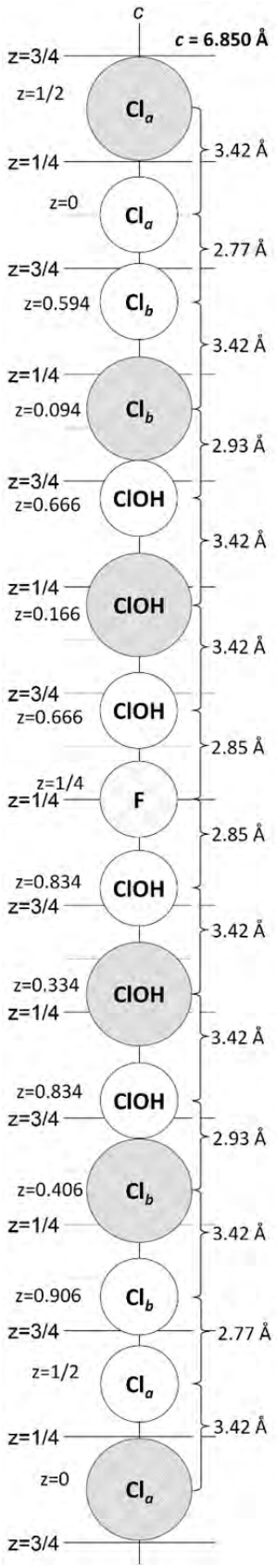

FIGURE 4. Sequence of atoms demonstrating a permissible reversal sequence of sites from above to below the mirror plane at z = 1/4 and z = 3/4 to maintain $P6_3/m$ symmetry in the Kurokura core apatite structure.

This is a preprint, the final version is subject to change, of the American Mineralogist (MSA)
Cite as Authors (Year) Title. American Mineralogist, in press.
(DOI will not work until issue is live.) DOI: http://dx.doi.org/10.2138/am-2017-5825

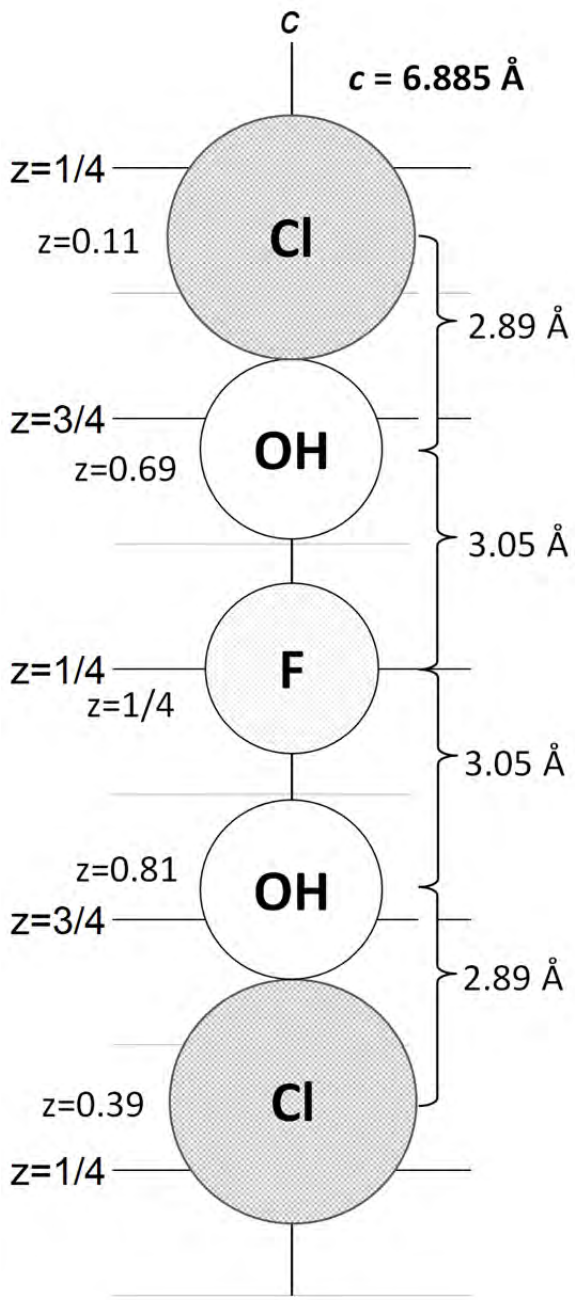

FIGURE 5. Sequence of atoms demonstrating a permissible reversal sequence of sites from above to below the mirror plane at z = 1/4 and z = 3/4 to maintain $P6_3/m$ symmetry in the Kurokura rim apatite structure.

This is a preprint, the final version is subject to change, of the American Mineralogist (MSA)
Cite as Authors (Year) Title. American Mineralogist, in press.
(DOI will not work until issue is live.) DOI: http://dx.doi.org/10.2138/am-2017-5825

TABLE 1. Electron microprobe chemical analysis of the Kurokura apatite. Each is an average of the three spots measured in the core and rim.

Oxide (wt.%)	Kurokura Core (n=3)			Kurokura Rim (n=3)		
CaO	53.404	±	0.328	54.998	±	0.363
F	0.716	±	0.134	1.843	±	0.689
Cl	3.244	±	0.055	0.848	±	1.005
P_2O_5	40.5	±	0.122	40.886	±	0.672
FeO	0.119	±	0.037	0.03	±	0.045
S	0.045	±	0.018	0.01	±	0.009
Nd_2O_3	0.291	±	0.048	0.136	±	0.042
Na_2O	0.168	±	0.03	0.036	±	0.052
SrO	0.024	±	0.003	0.018	±	0.005
Ce_2O_3	0.36	±	0.054	0.113	±	0.022
MnO	0.229	±	0.003	0.092	±	0.094
SiO_2	0.279	±	0.043	0.196	±	0.054
Dy_2O_3	0.051	±	0.031	0.042	±	0.024
Eu_2O_3	0.013	±	0.008	0.004	±	0.004
HO*	0.557	±	0.1	0.75	±	0.598
Total	100			100.002		
Apatite Structural Formula**						
Ca	9.659			9.792		
Na	0.055			0.012		
Fe	0.017			0.004		
Mn	0.033			0.013		
Sr	0.003			0.002		
Dy	0.003			0.002		
Eu	0.001			0.000		
Ce	0.022			0.007		
Nd	0.018			0.008		
Subtotal	9.810			9.840		
P	5.788			5.753		
Si	0.047			0.032		
S	0.014			0.003		
Subtotal	5.849			5.788		
Cl	0.928			0.240		
F	0.382			0.966		
OH*	0.664			0.875		
Subtotal	1.975			2.082		

*HO weight % and proportion in structural formula is calculated by difference.
**Apatite structural formula was calculated using atomic % values. Using net negative charge is problematic given OH substitution for F and Cl.

550 **TABLE 2.** Atomic coordinates and equivalent isotropic atomic displacement parameters (Å2) for

551 the Kurokura core sample.

552

Atom	x/a	y/b	z/c	U(eq)*
Ca1	2/3	1/3	0.99794(5)	0.01099(10)
Ca2	0.2417(4)	0.9969(3)	1/4	0.0076(3)
Ca2'	0.2676(4)	0.9946(5)	1/4	0.0076(3)
P	0.62949(4)	0.03123(4)	1/4	0.00684(9)
O1	0.51310(13)	0.84692(12)	1/4	0.01300(19)
O2	0.53517(14)	0.12404(13)	1/4	0.0165(2)
O3	0.73872(10)	0.08624(10)	0.06902(13)	0.02106(19)
F	0	0	1/4	0.0130(19)
ClB	0	0	0.0942(9)	0.0106(12)
ClOH	0	0	0.1662(10)	0.0159(12)
ClA	0	0	0	0.028(10)

*U(eq) is defined as one third of the trace of the orthogonalized U_{ij} tensor.

553

554

555 **TABLE 3.** Atomic coordinates and equivalent isotropic atomic displacement parameters (Å2) for

556 the Kurokura rim sample.

Atom	x/a	y/b	z/c	U(eq)*
Ca1	2/3	1/3	0.99875(5)	0.00896(8)
Ca2	0.2433(3)	0.99335(6)	1/4	0.0074(2)
Ca2'	0.275(6)	0.991(2)	1/4	0.0074(2)
P	0.63123(4)	0.02980(4)	1/4	0.00520(8)
O1	0.51536(13)	0.84289(13)	1/4	0.00972(19)
O2	0.53395(14)	0.12201(14)	1/4	0.0120(2)
O3	0.74258(10)	0.08495(10)	0.07029(12)	0.01393(16)
F	0	0	1/4	0.0097(14)
OH	0	0	0.193(3)	0.008(2)
Cl	0	0	0.113(13)	0.010(15)

*U(eq) is defined as one third of the trace of the orthogonalized U_{ij} tensor.

557

558

559

560 **TABLE 4.** Values of *z* for column anions in (0, 0, z) sites and percentage of total column anion
561 occupancy of each corresponding site for the core structural analysis of apatite from Kurokura.

Sample	F	% Sites	Cla	% Sites	Clb	% Sites	ClOH[1]	% Sites	Column Occupancy[2]
Kurokura Core	1/4	27.7	0	3.0	0.094	25.4	0.166	44.00	$F_{0.55}(OH)_{0.58}Cl_{0.87}$

[1]ClOH site: 65% OH, 35% Cl
[2]Constrained to 2.00 column anions/formula unit

562

563

564 **TABLE 5.** Values of *z* for column anions in (0, 0, z) sites and percentage of total column anion
565 occupancy of each corresponding site for the rim structural analysis of apatite from Kurokura.

566

Sample	F	% Sites	Clb	% Sites	OH	% Sites	Column occupancy
Kurokura Rim	1/4	52.6	0.113	2.1	0.193	51.0	$F_{1.05}(OH)_{1.02}Cl_{0.04}$

567

568

569

570

571

572

573

574

575

576

577

578

579

580

581